Reversible Coloration Enhanced by Electrochemical Deposition of an Ultrathin Zinc Layer onto an Anodic Nanoporous Alumina Layer

Shuzo Hirata, Toshiro Tsuji, Yoshimine Kato, and Chihaya Adachi**

A productive method is introduced to realize large area color electronic paper (e-paper) with high UV resistance, heat resistance, and good significant bending properties using a color change triggered by reversible electronic change in the device structure. Reversible coloration and decoloration triggered by electrochemical deposition and desorption, respectively, of an ultrathin zinc (Zn) layer on a thin transparent conductive layer coated on anodic nanoporous alumina has been developed. The deposition of the ultra-thin Zn layer triggers the formation of destructive interference, which leads to coloration. Yellow, magenta, and cyan colors were obtained in the colored state by increasing the NP-Al_2O_3 layer thickness, based on Bragg diffraction theory. Reflectance of more than 70% and contrast values of more than 7 were obtained, which are nearly equivalent to those of previous e-papers. The color images in these devices also showed high UV resistance, heat resistance, and repeated significant bending endurance. The devices can be fabricated with large areas using low-cost manufacturing processes such as anodic oxidation, and use abundantly available materials. Our proposed device provides low-cost and flexible large area color e-paper for outdoor use.

1. Introduction

Electronic paper (e-paper) is a type of display that realizes ecologically friendly static images, because it requires no electrical power to maintain these images.[1] The electrostatic transportation of electrically-charged particles such as bichromal balls,[2] microcapsule-type electrophoretic particles,[3] and charged electronic liquid powders[4] has been reported as a system that allows e-papers to realize reversible static black and white images. Electrochemical deposition and desorption of a silver layer on titanium oxide particles has also been reported as an e-paper system to realize reversible static black and white images.[5] However, there is a problem in that the static images formed using these electrically-charged particles are not stable after repeated significant bending of the e-paper.[6] The reversible static black and white images also need color filters to display the image colors, but these color filters may potentially become decolored after long-term irradiation with ultraviolet (UV) light, which intrinsically makes it difficult to use these e-papers for outdoor applications.

For reversible coloration and decoloration without using color filters, techniques based on the electrochromism of organic dyes have been reported.[7–11] However, organic dyes are not typically stable under long-term UV light irradiation and high temperatures. Although methods based on the electrochromism of metal oxides have been reported,[12] their response times in device applications have not been good enough for practical use. Color images using the transportation of charged oil have also been reported,[13–15] but the images using colored oils are potentially unstable under significant repeated bending conditions. The orientation control of liquid-crystalline materials with memory functions in three stacked layers has also been reported as a method to obtain full color static images without using color filters.[16] However, the complex stacked structure of the device is not suitable for low-cost manufacture and the orientation of the liquid-crystalline molecules is sensitive to significant device bending, causing the static images to break after repeated significant bending.[17] The narrow temperature range of the cholesteric liquid crystalline state also makes it impossible to drive such a device under higher temperature conditions, making it difficult to use these e-papers in outdoor applications. If color e-papers with not only high reflectance and high contrast, but also high UV resistance, heat resistance, and good significant bending properties can be developed, they can be used to provide flexible color e-papers for outdoor use.

One promising technique that can be used to realize intrinsically high UV resistance, heat resistance, and good significant bending properties in e-papers is the use of a color change caused by a change in optical interference triggered by a reversible electronic change in the device structure.[18,19] In this paper, we demonstrate a new reversible coloration and decoloration system using the changes in optical interference triggered by the electrochemical deposition and

Dr. S. Hirata, Prof. C. Adachi
Center for Organic Photonics
and Electronics Research (OPERA)
Kyushu University
744 Motooka, Nishi, Fukuoka 819-0395 Japan
E-mail: hirata@cstf.kyushu-u.ac.jp;
adachi@cstf.kyushu-u.ac.jp
T. Tsuji, Prof. Y. Kato
Department of Automotive Science
Kyushu University
744 Motooka, Nishi, Fukuoka 819-0395 Japan

DOI: 10.1002/adfm.201200353

desorption of an ultra-thin zinc (Zn) layer on a thin transparent conductive layer (TCL) coated on an anodic nanoporous alumina[20–22] (NP-Al_2O_3) layer. The proposed devices can be manufactured quickly at low cost using conventional electroplating processes such as anodic oxidation and using low-cost materials. Reflectance of more than 70% and contrast values larger than 7 were achieved, which are among the highest reported reflectance and contrast values for e-papers.[23] Reversible coloration and decoloration of cyan, magenta, and yellow were achieved by changing the thickness of the anodic NP-Al_2O_3 layer. The recorded images did not disappear when the electrical power was removed. Also, the recorded color of the device hardly changed when the device was significantly tilted (see movie S1 in the Supporting Information). This mechanism of electrical coloration and decoloration is useful for large area color e-papers with not only high reflectance and contrast, but also high UV resistance and heat resistance. The colored state of the device is also stable after repeated significant bending.

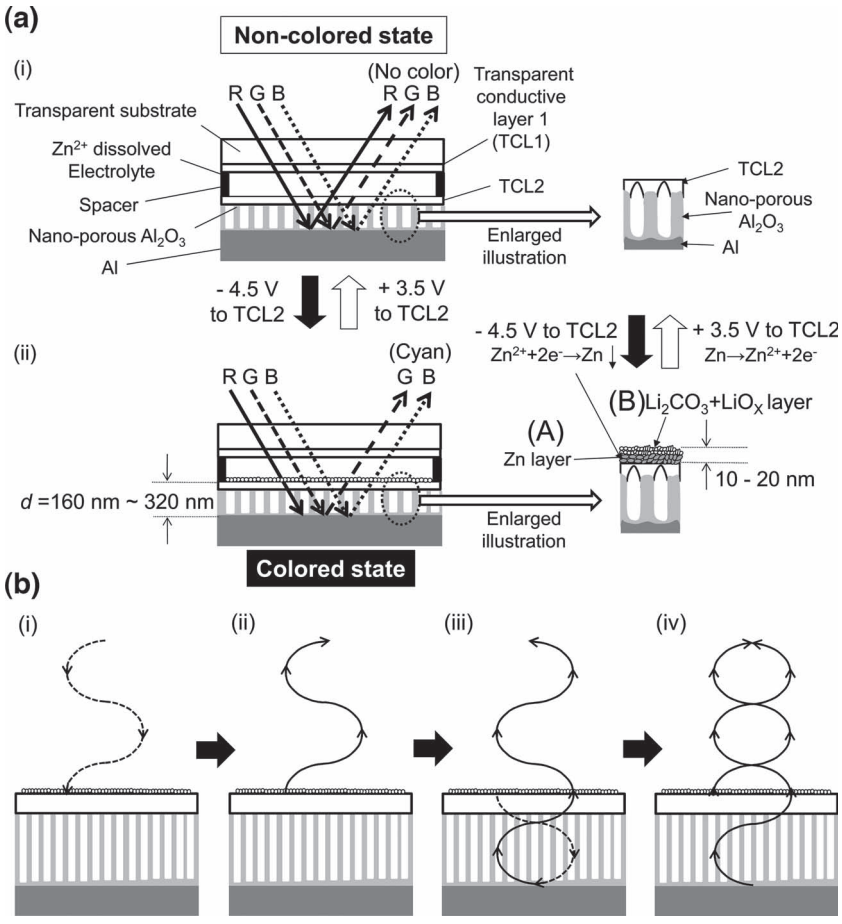

Figure 1. Mechanisms of coloring and decoloring in the devices reported in this research: (a) Reversible structural changes in non-colored state (i) and colored state (ii). In the non-colored state, the device structure is TCL1/electrolyte containing Zn^{2+} ions/TCL2/NP-Al_2O_3/Al. In the colored state; the device structure is TCL1/electrolyte containing Zn^{2+} ions/Li_2CO_3+LiO_X/Zn/TCL2/NP-Al_2O_3/Al. (b) Explanation of decreased reflectance at a specific wavelength after electrodeposition of Zn layer with thickness of several nm on TCL2.

2. Mechanism of Coloration and Decoloration

The coloration and decoloration mechanisms of the proposed device must now be explained. **Figure 1**a shows the basic structure in the non-colored state of the device, which is: transparent conductive layer 1 (TCL1)/electrolyte layer, composed of 0.2 M $LiClO_4$, 1.0 wt% $ZnCl_2$, and propylene carbonate (50 μm)/transparent conductive layer 2 (TCL2) (30 nm)/NP-Al_2O_3 (*X* nm)/Al. In the state of Figure 1a(i), no color is observed because red-green-blue (RGB) lights are reflected at the Al layer. The colored state is recorded by the application of a positive bias to TCL2 for a few seconds (see Supporting Information, movie S2). When the positive bias is applied to TCL2, an ultra-thin Zn layer is deposited on TCL2 by electrochemical reduction from Zn^{2+} ions contained in the electrolyte layer (inset (A) of Figure 1a(ii)). Although the Zn layer is usually oxidized in air, Li was automatically deposited from Li^+ contained in the electrolyte layer on the Zn layer within a few seconds, and was oxidized to give a mixed layer composed of Li_2CO_3 and LiO_X (inset (B) of Figure 1a(ii)). The mixed layer protects the Zn layer from the oxygen in the air. This Zn layer covered with the Li_2CO_3 and LiO_X mixed layer acts as a semi-transparent mirror. In this state, part of the incident light at a specific visible wavelength (λ_{WR}) irradiated on the device (dashed line of Figure 1b(i)) is reflected without a phase shift at the interface between the electrolyte layer and the Zn layer, forming a wave as shown in the fine line of Figure 1b(ii). Another part of the incident light at λ_{WR} penetrates into the Li_2CO_3 and LiO_X covered Zn layer (dashed line of Figure 1b(iii)). It is then reflected without a phase shift at the Al layer, forming a wave as shown in the fine line of Figure 1b(iii). The two reflected waves shown in the fine lines of Figures 1b(ii) and (iii) are completely out of phase and destructively interfere, because the phase difference between the two reflected waves always has a value of π (Figure 1b(iv)). Consequently, the reflectance spectrum of the device was significantly decreased around λ_{WR}, resulting in the observance of the colored state. The non-colored state is recovered by application of a positive bias to TCL2 within 20 ms (see supporting movie S3). When the positive bias is applied to TCL2, the device structure shown in Figure 1a(ii) returns to the condition shown in Figure 1a(i) by desorption of the Zn layer into the electrolyte layer, and results in the device returning to a non-colored state. The coloration and decoloration can be repeated using the reversible structural changes shown in Figure 1a(i) and (ii) because of the electrochemical deposition and desorption of the ultra-thin Zn layer on TCL2, respectively.

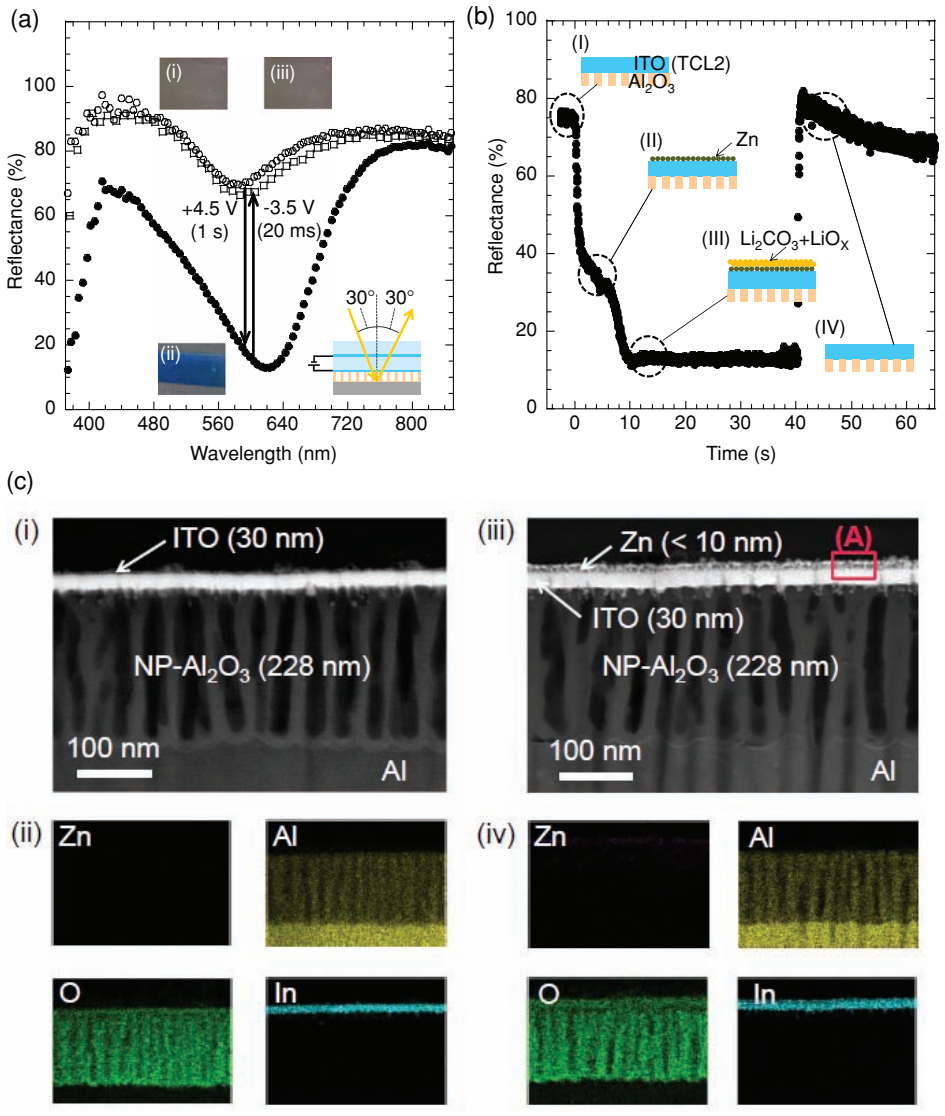

Figure 2. Reversible spectral and structural changes of a proposed device with a 235 ± 5 nm-thick NP-Al_2O_3 layer (device III): (a) Reflectance spectral changes before coloration (open circles), after coloration (solid circles), and second decoloration (open squares) when the incident and detection angles are 30°. The inset photographs (i), (ii), and (iii) show the coloring conditions of the devices before and after coloration, and after second decoloration, respectively. The inset figure illustration explains the reflectance measurement. (b) Cross-sectional transmission electron microscope (TEM) images ((i) and (iii)) and elemental analysis images ((ii) and (iv)) in the non-colored and colored states, respectively. (c) Reflectance changes at 620 nm during the coloration and decoloration processes. The –4.5 V potential was applied to TCL2 from 0 to 5 s. A positive 3.5 V potential was applied to TCL2 at 40 s .

3. Results and Discussion

3.1. Demonstration of Coloration and Decoloration

Figure 2 shows the structural and reflectance changes of device III with a 235 ± 5 nm thick-NP-Al_2O_3 layer before and after the coloring process, and after the second decoloration process when indium-tin oxide (ITO) was used as the material for TCL1 and TCL2. Before the application of a negative bias to the ITO layer as TCL2, no Zn layer was observed on the ITO layer (Figure 2c(i) and (iii)). In this state, lights in RGB colors were reflected at the Al layer because no precipitate had been deposited on the ITO TCL2, resulting in the non-colored state of the device (open circles in Figure 2a). Reflectance of higher than 70% was obtained in the non-colored state. When –4.5 V was applied to the ITO TCL2 electrode for 5 s, an ultra-thin Zn layer with a thickness of several nm was deposited on the ITO/NP-Al_2O_3 layer, as shown in Figure 2c(iii) and (iv). In this state, only red light cannot be reflected from the device, forming cyan color (solid circles in Figure 2a). The reflectance at 621 nm was 10% in the colored state. The deposition of the ultra-thin Zn layer occurs during the application of –4.5 V to TCL2, which

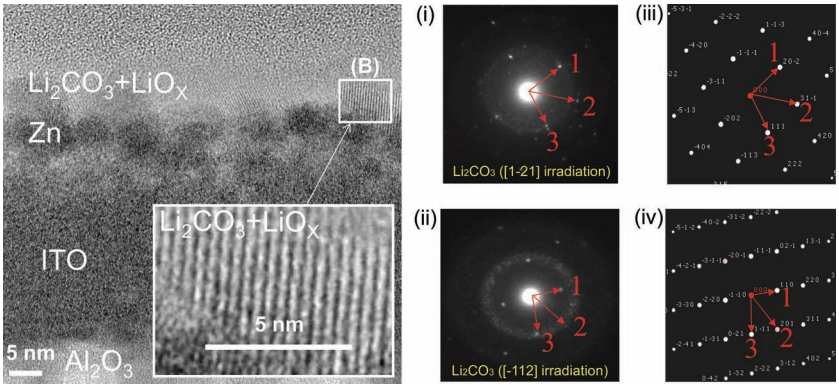

Figure 3. Surface analysis of TCL2 in a proposed device with a 235 ± 5 nm-thick NP-Al_2O_3 layer (device III) in colored state: (a) Enlarged TEM images at point (A) in Fig 2b(iii). (b) Electron beam diffraction patterns at point (B) in Figure 2d. (i) and (ii) are the experimental and theoretical diffraction patterns of Li_2CO_3 for the case of [1–21] irradiation, respectively. (iii) and (iv) are the experimental and theoretical diffraction patterns of Li_2CO_3 for the case of [–112] irradiation, respectively.

was observed as a decrease in the reflectance from 0 s to 5 s in (II) of Figure 2b. After the deposition of an ultra-thin Zn layer, a mixed layer composed of Li_2CO_3 and LiO_X was deposited automatically on the Zn layer from Li^+ ions in the electrolyte layer within a few seconds, as shown in the results of the electron diffraction analysis of **Figure 3** and by X-ray photoelectron spectroscopy (XPS) (see Figure S1 of the Supporting Information). The formation of the mixed layer composed of Li_2CO_3 and LiO_X can be observed as a small decrease in reflectance from 5 s to 10 s as shown in (III) of Figure 2b. The mixed layer of Li_2CO_3 and LiO_X protects the semi-transparent Zn layer from oxidation because the colored state disappeared within several seconds, because of oxidation of the Zn layer when $LiClO_4$ was not doped into the electrolyte. The colored state showing cyan color was stable at room temperature (RT) in air for at least six months without any applied electrical power. However, the colored state disappears and is converted into the non-colored state within 20 ms (open squares in Figure 2a and (IV) of Figure 2b) because the ultra-thin Zn layer and the mixed layer of Li_2CO_3 and LiO_X dissolved into the electrolyte layer when a positive voltage of 3.5 V was applied to the ITO TCL2 (inset (iii) of Figure 2c). The non-colored state was also stable at RT in air for a long time without any applied electrical power. Although ITO was used for TCL2 for easy observation of the deposition of the ultra-thin Zn layer by energy dispersive X-ray spectrometry (EDS), we noted that reversible coloration and decoloration were observed when alumina-zinc oxide (AZO ($ZnO:Al_2O_3$)) or a transparent conducting polymer such as poly(3,4-ethylenedioxythiophene)poly(styrenesulfonate) were used for TCL1 and TCL2. These results therefore indicate that the proposed device is suitable for area color e-papers, which can only be constructed using abundant materials.

3.2. Color Tuning in the Colored State

The colors of the colored state can be changed by controlling the total thickness of TCL2 and the NP-Al_2O_3 layer (d). **Figure 4**a shows the reflectance spectra of three types of e-papers, which are devices I, II, and III, in both the non-colored and colored states. The colors in the colored states of devices I, II, and III were yellow, magenta, and cyan, respectively. The thickness values of d in devices I, II, and III were 189 ± 5 nm, 228 ± 5 nm, and 265 ± 5 nm, respectively (Figure 4b). Figure 4b also indicates that the wavelength showing the weakest reflectance in the colored state (λ_{WR}) was shifted to longer wavelengths with increasing thickness of the NP-Al_2O_3 layer (X). Also, λ_{WR} was almost proportional to d (=$30 + X$ nm, where 30 nm is the thickness of ITO used for TCL2) as shown in the dashed line of Figure 4b. These results can be explained by using the destructive interference in Bragg's law and λ_{WR} was expressed by the following equation.

$$\lambda_{WR} = 4nd/\left[(2m + 1)\cos\theta\right] (m = 0, 1, 2, 3, \ldots) \quad (1)$$

where n is the average refractive index of the layer composed of TCL2 and the NP-Al_2O_3 layer, and θ is the angle of the incident light relative to the substrate. The result of positive proportionality between λ_{WR} and d therefore indicates that the coloration of the e-paper depends on Bragg's diffraction theory based on Equation 1. Figure 4a also shows that the λ_{WR} values of the devices showing cyan color in the colored state are 373 nm and 621 nm, corresponding to the cases where $m = 1$ and $m = 0$ in the theory of Equation 1, respectively.

In the colored state, the color became obscured with increasing d. When the number m is increased with increasing d, many types of interfering waves were formed in the reflectance

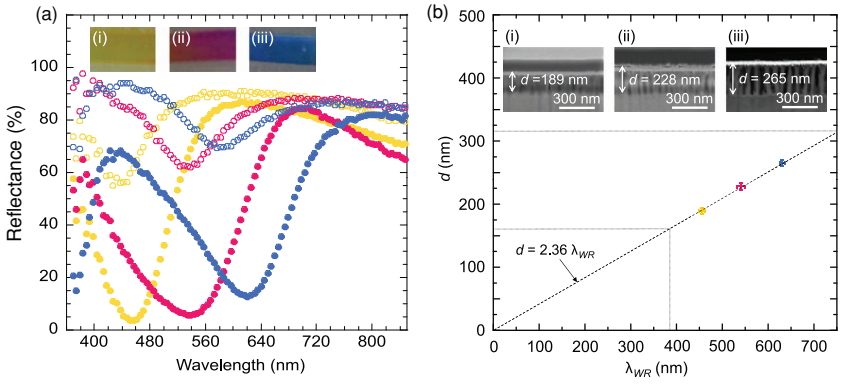

Figure 4. Color changes in the colored state depending on the difference in the total thickness of the ITO layer and the NP-Al_2O_3 layer: (a) Reflectance spectra of devices I (yellow), II (magenta), and III (cyan) in non-colored state (open plots) and colored state (solid plots) when the incident and detecting angles are both 30°. (b) Relationship between d and λ_{WR}. Black dashed line indicates $\lambda_{WR} = 2.36d$. Insets (i), (ii), and (iii) are cross-sectional scanning electron microscope (SEM) images of devices I, II, and III, respectively.

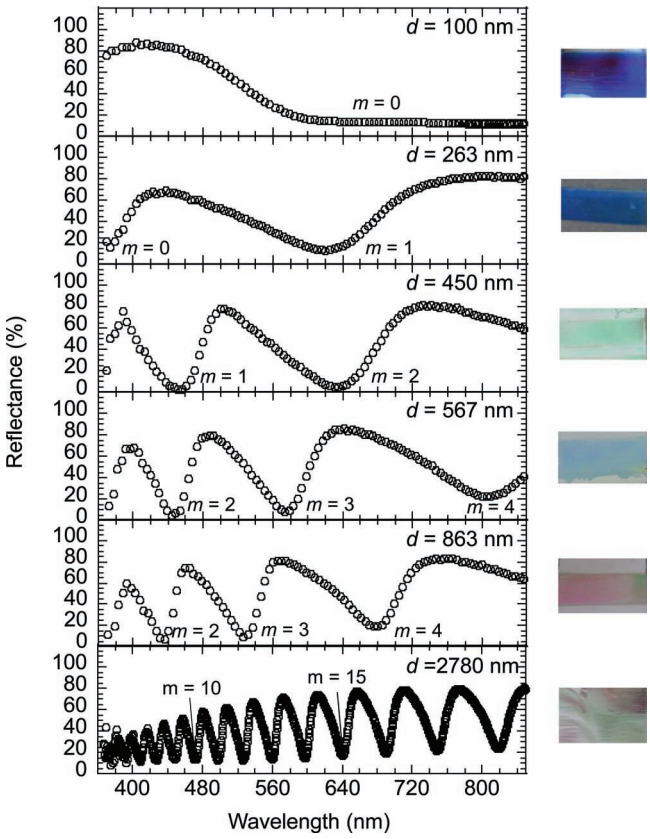

Figure 5. Difference in reflectance spectra in colored state depending on changes of *m* numbers with increasing *d*: Device structures in the colored state are ITO/electrolyte/electrodeposited Zn (several nm)/ITO (30 nm)/NP-Al_2O_3 (*d* - 30 nm)/Al. The total thickness of the ITO layer and the NP-Al_2O_3 layer (*d*) in the devices was changed by changing the time of anodic oxidation. The incident and detection angles used to measure the reflectance spectra are 30°.

spectra of the colored state, as shown in **Figure 5**. This causes mixing of various colors at the same time, obscuring coloration in the colored state as shown in the inset photos of Figure 5. Therefore, the fabrication of a device with the condition $m = 1$ at λ_{WR} is desirable to obtain a clear color in the colored state, meaning that the *d* value is limited from 161 nm to 318 nm, as shown in Figure 3b when λ_{WR} should be located at the visible wavelength from 380 nm to 750 nm.

3.3. Comparison of Experimental Data with Theoretical Data Based on Theory of a Destructive Mode in an Optical Interference Coating

The use of a material with the appropriate refractive index and extinction coefficient as the electrodeposited layer is necessary to obtain a clear color in the colored state. **Figure 6**a indicates the difference in the reflectance spectra for the case of $\theta = 0$ when different types of materials were used for the electrodeposited layer. Although electrodeposition of silver (Ag) and Zn onto an ITO (30 nm)/NP-Al_2O_3 (198 ± 5 nm)/Al structure resulted in a large decrease in reflectance at λ_{WR}, deposition of N,N′-bis(naphthalen-1-yl)-N,N′-bis(phenyl)-benzidine (α-NPD) onto an ITO (30 nm)/NP-Al_2O_3 (198 ± 5 nm)/Al structure did not show decreased reflectance at λ_{WR}. The half width at half-maximum of a reflectance decrease at λ_{WR} in the case of $\theta = 0$ ($\Delta\lambda_{WR}$) and reflectance at λ_{WR} in the case of $\theta = 0$ (R) depend on the refractive index of the Al layer (n_1), the extinction coefficient of the Al layer (k_1), the refractive index of the electrodeposited layer (n_2), the extinction coefficient of the electrodeposited layer (k_2), and the average refractive index of the ITO/NP-Al_2O_3 layer (n). R and $\Delta\lambda_{WR}$ are expressed using n_1, k_1, n_2, k_1, and n in the following equations.

$$\Delta\lambda_{WR} \propto (1 - r_1 r_2)/(r_1 r_2)^{1/2} \quad (2)$$

$$r_1 = \left|(n_1 - k_1 i - n)/(n_1 + k_1 + n)\right| \quad (3)$$

$$r_2 = \left|(n_2 - k_2 i - n)/(n_2 + k_2 i + n)\right| \quad (4)$$

$$R = (r_1^2 + r_2^2 + 2r_1 r_2 \cos\Phi)/(1 + (r_1 r_2)^2 + 2r_1 r_2 \cos\Phi) \quad (5)$$

$$\Phi = 4\pi nd/([2m + 1]\lambda)\,(m = 0,\ 1,\ 2,\ 3,\ \ldots) \quad (6)$$

where λ is the wavelength. These equations are based on the theory of a destructive mode in an optical interference coating such as a Rayleigh film.[24] The theoretical relationships of R and $\Delta\lambda_{WR}$ for Ag, Zn, Al, and α-NPD that were calculated by substituting theoretical values of n_2 and k_2 for Ag, Zn, Al, and α-NPD into equations 2 to 6 (Figure 6b) showed similar tendencies to the experimental relationships (Figure 6a). Therefore, the appropriate electrodeposited material for efficient coloration in the colored state can be estimated using equations 2 to 6. Based on equations 2 to 6, larger values of k_2 and smaller values of n_2 are required to obtain a large decrease in reflectance at λ_{WR} in the colored state (see Figure S2 of the Supporting Information). A large decrease in reflectance cannot be obtained for the cases of organic materials and metal oxides because k_2 is too small (for the case of α-NPD shown in Figure 6). However, many metals meet the requirements that n_2 is smaller than 1.0 and k_2 is large. However, the electrochemical deposition of Al and Pt on TCL2 can not occur at RT,[25] precluding reversible coloration and decoloration. Gold (Au) has the problems of high cost and material scarcity when compared with Zn. Au and copper (Cu) have the problem of self-coloration, which interferes with the non-colored state of the device. Although clear coloration was obtained when Ag was used as the metal, the colored state was unstable and erased gradually at RT. However, Zn fulfills all of the required conditions, not only having a large decrease in reflectance in the colored state, but also being a low-cost and abundant material. Although Zn is not stable in air, the mixed layer of Li_2CO_3 and LiO_X formed by deposition and oxidation on the Zn layer suppresses oxidation of the Zn layer, resulting in a long-term stable colored state. Zn is therefore the most suitable element for the electrodeposited material in our proposed device.

3.4. Color Stability under Heating, UV irradiation, and Repeated Significant Bending

The most important advantage of the device shown in Figure 1 compared to conventional devices is that the static images are

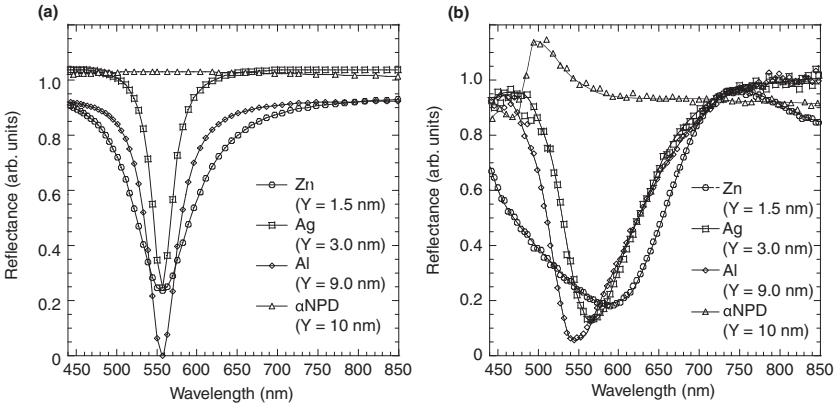

Figure 6. Differences in reflectance spectra in colored state when different materials were used for the electrodeposited layer: Zn, Ag, Al, and α-NPD were used as the electrodeposited layers. Reflectance spectra in the non-colored state were normalized to 1.0. (a) Experimental reflectance spectra in the colored state relative to reflectance spectra in the non-colored state. The device structure is deposited layer (Zn, Ag, Al, or α-NPD) (Y nm)/ITO (30 nm)/NP-Al_2O_3 (198 ± 5 nm)/Al. The Zn layer was prepared on the ITO layer by electrodeposition, as shown in the experimental section. The Ag, Al, and α-NPD layers were prepared by vacuum deposition on the ITO layer. (b) Theoretical reflectance spectra in the colored state relative to reflectance spectra in the non-colored state. A structure of deposited layer (Y nm)/transparent layer with n = 1.53 (233 nm)/Al was used for the calculation. n_1 and k_1 values at 550 nm for Al are 0.9 and 6.7, respectively. n_2 and k_2 values for Zn, Ag, Al, and α-NPD at 550 nm are 2.4 and 5.5, 0.1 and 3.3, 0.9 and 6.7, and 1.5 and 0, respectively. The incident and detection angles used to measure the reflectance spectra are 0°.

significantly stable under heating, strong UV irradiation, and repeated significant bending. **Figure 7**a(i) shows the reflectance change at λ_{WR} of device III shown in Figure 2 when it was placed on a hot plate at 80 °C. The color of the device was erased gradually with increasing temperature because of gradual oxidation of the Zn layer when the surface of the Zn layer in the device was exposed in air without any sealing layer.

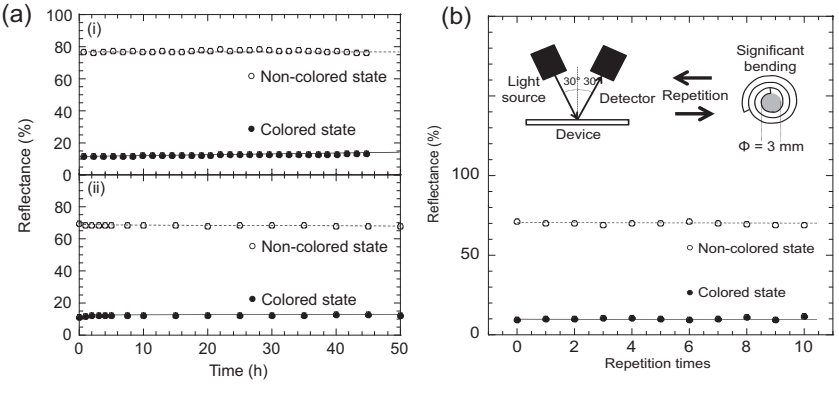

Figure 7. Stability of static color images: (a) Reflectance changes in the non-colored state and the colored state when a device was heated at 80 °C for 50 h (i) and when the device was irradiated with UV light at 365 nm with 1 mW/cm^2 at RT for 50 h (ii). A glass (0.7 mm)/ITO (100 nm)/electrolyte (50 μm)/ITO (30 nm)/NP-Al_2O_3 (248 ± 5 nm)/Al (300 μm) (device III) structure was used to evaluate heat and UV resistance. (b) Reflectance changes in the non-colored state and the colored state when the device was repeatedly bent under the condition of Φ = 3 mm. A PET (25 μm)/ITO (100 nm)/electrolyte (50 μm)/ITO (30 nm)/NP-Al_2O_3 (248 ± 5 nm)/Al (50 μm) structure was used to evaluate the stability of the static color images after each bending incidence.

On the other hand, the reflectance in both the non-colored and colored states increased after long-term heating when the device was sealed using an epoxy resin. Figure 7a(ii) shows that the reflectance of device III did not change when the device was irradiated with strong UV light. These results indicate that the proposed device can be used in outdoor environments for a long time. This is because the coloring mechanism is not based on the absorption of the materials, but on destructive interference using structural changes in the device. Figure 7b shows no reflectance changes at λ_{WR} for the device in the colored state when it was repeatedly bent. This result is much better than those of e-papers using electrically-charged particles[4] or cholesteric liquid crystals.[16,17] The preservation of the stable image after significant bending is ascribed to no change occurring in the d value because the colored state of the device is ascribed to the distance between the electrodeposited layer and the Al substrate. Our proposed device is therefore suitable for area color e-papers with good flexibility properties.

4. Conclusions

We have demonstrated reversible coloration and decoloration triggered by electrochemical deposition and desorption, respectively, for an ultra-thin Zn layer on a TCL/anodic NP-Al_2O_3 layer on an Al substrate. The deposition of the ultra-thin Zn layer with a thickness of several nm on the TCL/NP-Al_2O_3 layer triggers the formation of destructive interference, which in turn leads to coloration. Yellow, magenta, and cyan colors could be obtained in the colored state by increasing the total thickness of the TCL layer and the NP-Al_2O_3 layer, based on Bragg diffraction theory. Reflectance of more than 70% and contrast values larger than 7 were obtained. The color images in the devices also showed high UV resistance, heat resistance, and endurance to repeated significant bending. The devices could be fabricated with large areas using low-cost manufacturing processes such as anodic oxidation and used abundantly available materials. Our proposed device is applicable to low-cost flexible area color e-papers with high UV resistance and heat resistance.

5. Experimental Section

Anodic NP-Al_2O_3 structures were prepared on an Al substrate according to previously reported procedures.[21,22] In a typical process, an Al sheet (99.99% purity, thickness of 50 μm or

300 μm, supplied by Furuuchi Chem.) was electropolished in a solution composed of perchloric acid and ethanol after degreasing in acetone. The Al surface was anodized in a 1.0 wt% H_2SO_4 solution at RT under a constant voltage of 20 V at RT for 2 h. After the first anodization, the oxide layer was removed using a solution of 1.8 wt% chromic acid and 6.0 wt% phosphoric acid. The second Al anodization was carried out under a constant voltage of 20 V in a 1.0 wt% H_2SO_4 solution at RT for 300 s (device I), 420 s (device II), and 540 s (device III), giving NP-Al_2O_3 structures on the Al substrate. After the second anodization, pore-widening treatment of the NP-Al_2O_3 structure was carried out in 5.0 wt% phosphonic acid at 30 °C for 15 min. Then, ITO was deposited as TCL2 on the anodic NP-Al_2O_3 layer by radio frequency (RF) sputtering at a speed of 0.04 nm s^{-1}, giving a TCL2/NP-Al_2O_3/Al structure. The TCL1 side of a TCL1 coated glass or polyethylene terephthalate (PET) substrate and the TCL2 side of the TCL2/NP-Al_2O_3/Al substrate were connected to each other using a thermosetting resin adhesive sheet (Himilan, Mitsui Polychemicals) while maintaining a gap of approximately 50 μm. The e-paper structure was completed by insertion of an electrolyte composed of 0.2 M $LiClO_4$, 1.0 wt% $ZnCl_2$, and propylene carbonate as a solvent. Finally, all of the side areas of the device were completely sealed using an epoxy resin (T693/4000, Nagase Chemtex) and the epoxy resin was completely cured by UV light irradiation. The active area of the devices was 5 mm ×10 mm. All devices were fabricated under the same atmosphere.

Reflectance spectral changes in the non-colored and colored states were measured using an optical system combining a halogen lamp (HL-2000, Ocean Optics) as a light source and an integrated sphere attached to a multichannel spectrometer (PMA11, Hamamatsu Photonics Co.) as a detector. A hotplate (NA-1, Ninos) and a UV light from the excitation unit of a spectrofluorometer (F560, Jasco) were used to measure the heat resistance and UV resistance of the static images in a device, respectively. Cross-sectional images were measured by field-emission transmission electron microscopy (HF-2000, Hitachi) and field-emission scanning electron microscopy (S-5500, Hitachi High Tech.). Elemental analysis of the cross-sectional view of the device was carried out by EDS (System Six, Noran). Surface analysis of the electrodeposited materials on TCL2 was carried out by XPS (Quantera SXM, Physical Electronics) and electron diffraction analysis (HF-2000, Hitachi).

Supporting Information

Supporting Information is available from the Wiley Online Library or from the author.

Acknowledgements

We thank Kobelco Research Institute Inc. for observation of the cross-sectional TEM images, SEM images, and EDS analysis of the devices. This work was supported by the Adaptable and Seamless Technology Transfer Program through Target-driven R&D (AS231Z01236B), the New Energy and Industrial Technology Development Organization (NEDO), a Grant-in-Aid for Young Scientists (B) (22750132) from the Japan Science and Technology Agency, a Grant-in-aid from the Funding Program for World-Leading Innovative R&D on Science and Technology (FIRST), and the Global COE Program, "Science for Future Molecular Systems" from the Ministry of Education, Culture, Sports, Science, and Technology of Japan.

Received: February 6, 2012
Published online: June 12, 2012

[1] J. Heikenfeld, P. Drzaic, J. Yeo, T. Koch, *J. Soc. Inf. Display* **2011**, *19*, 129.
[2] M. J. Crowley, K. N. Sheridon, L. Romano, *J. Electrostatics* **2002**, *55*, 247.
[3] B. Comiskey, J. D. Albert, H. Yoshizawa, J. Jacobson, *Nature* **1998**, *394*, 253.
[4] R. Hattori, S. Yamada, Y. Masuda, N. Nihei, R. Sakurai, *J. Soc. Inf. Display* **2004**, *12*, 75.
[5] K. Shinozaki, *J. Soc. Inf. Display* **2002**, *33*, 39.
[6] It has been reported that images on the device shown in ref. 4 were not destroyed after repeated bending with a bend radius of $\Phi = 20$ mm.
[7] P. Bonhote, E. Gogniat, F. Campus, L. Walder, M. Graetzel, *Displays* **1999**, *20*, 137.
[8] U. Bach, D. Corr, D. Lupo, F. Pichot, M. Ryan, *Adv. Mater.* **2002**, *14*, 845.
[9] P. M. Beaujuge, S. Ellinger, J. R. Reynolds, *Adv. Mater.* **2008**, *20*, 2772.
[10] Y. Kondo, H. Tanabe, H. Kudo, K. Nakano, T. Otake, *Materials* **2011**, *4*, 2171.
[11] P. M. Beaujuge, S. V. Vasilyeva, D. Y. Liu, S. Ellinger, T. D. McCarley, J. R. Reynolds, *Chem. Mater.* **2012**, *24*, 255.
[12] S. Gottesfeld, J. D. E. McIntyre, *J. Electrochem. Soc.* **1979**, *126*, 742.
[13] R. A. Haynes, B. J. Feenstra, *Nature* **2003**, *425*, 383.
[14] J. Heikenfeld, K. Zhou, E. Kreit, B. Raj, S. Yang, B. Sun, A. Milarcik, L. Clapp, R. Schwartz, *Nat. Photonics* **2009**, *3*, 292.
[15] S. Yang, K. Zhou, E. Kreit, J. Heikenfeld, *Appl. Phys. Lett.* **2010**, *97*, 143501.
[16] T. Yoshihara, J. Tomita, Y. Shinkai, *FUJITSU* **2006**, *57*, 302, in Japanese.
[17] Color images on the device shown in ref. 16 were not destroyed after bending with a radius of $\Phi = 60$ mm.
[18] M. Miles, E. Larson, C. Chui, M. Kothari, B. Gally, J. Batey, *J. Soc. Inf. Display* **2003**, *11*, 209.
[19] B. J. Gally, *J. Soc. Inf. Display Symposium Digest of Technical Papers* **2004**, *35*, 654.
[20] H. Masuda, K. Fukuda, *Science* **1995**, *268*, 1466.
[21] H. Masuda, M. Satoh, *Jpn. J. Appl. Phys.* **1996**, *35*, L126.
[22] H. Masuda, M. Nagae, T. Morikawa, K. Nishio, *Jpn. J. Appl. Phys.* **2006**, *45*, L406.
[23] The reflectance performance of previous e-papers was summarized in the introduction of ref. 14.
[24] F. L. Pedrotti, L. M. Pedrotti, L. S. Pedrotti, *Introduction to Optics*, Prentice Hall, 3rd edition, **2007**.
[25] No references for electrodeposition of Al and Pt at RT were found. Electrodeposition of Al was often carried out using melted Al at about 700 °C.